# EXPERIMENTAL INVESTIGATION OF CONTROL ABSORBER BLADE EFFECTS IN A MODERN 10X10 BWR ASSEMBLY

*F. Jatuff, P. Grimm, M. Murphy, A. Lüthi, R. Seiler, O. Joneja, A. Meister,*
*R. van Geemert, R. Brogli, R. Chawla (PSI), T. Williams (EGL) and S. Helmersson (Westinghouse)*

*The accurate estimation of reactor physics parameters related to the presence of cruciform absorber blades in Boiling Water Reactors (BWRs) is important for safety assessment, and for achieving a flexible operation during the cycle. Characteristics which are affected strongly include the power distribution for controlled core regions and its impact on linear heat generation rate margins, as well as the build-up of plutonium, and its influence on core excess reactivity and the reactivity worth of the shutdown system. PSI and the Swiss Nuclear Utilities (UAK) are conducting an experimental reactor physics programme related to modern Light Water Reactor (LWR) fuel assemblies, as employed in the Swiss nuclear power plants: the so-called LWR-PROTEUS Phase I project. A significant part of this project has been devoted to the characterization of highly heterogeneous BWR fuel elements in the presence of absorber blades. The paper presents typical results for the performance of modern lattice codes in the estimation of controlled assembly reaction rate distributions, the sensitivity to the geometrical and material characterization, and a preliminary comparison of reflected-test-zone calculations with experimental reaction rate distributions measured in a Westinghouse SVEA-96+ assembly under full-density water moderation conditions in the presence of Westinghouse boron-carbide absorber blades.*

## 1 INTRODUCTION

Current trends in BWR fuel technology are motivated by the enhancement of safety assessments, and the improvement of the overall performance, which includes the increase of the discharge burn-up, longer operating cycles, power up-rate, and plant life extension. These trends have resulted in ever-more heterogeneous fuel assembly designs, presenting high average $^{235}U$ enrichments, many different fuel rod types, an increasing number of burnable absorber fuel rods and sophisticated internal water regions. Such design sophistication aims at the continued increase of maximum channel powers, maximum burnup, and further flattening of the assembly power distribution.

One of the most significant reactor physics research initiatives supporting these trends is the LWR-PROTEUS Phase I project [1] carried out at PSI in close co-operation with the Swiss Nuclear Utilities. This project has been designed to (a) evaluate the capabilities of different modern calculational codes of interest to the Swiss utilities using nominal assembly data (*production models*), (b) qualify the adequacy of *production models* by studying the sensitivity of reactor physics parameters with regard to departure from nominal conditions (geometry and material characterization), and (c) validate these codes by developing an ambitious experimental programme, which includes the measurement of rod-by-rod reaction rate distributions, individual fuel rod reaction rate ratios, and the reactivity effects of perturbing a critical lattice by removing individual fuel rods. The experiments use actual, modern LWR fuel under different operational conditions [2].

One important part of the investigation is related to the study of strongly perturbed fuel assemblies, as produced by introducing absorber blades in the inter-assembly gaps. The presence of cruciform absorber blades inserted from the bottom of the reactor pressure vessel in BWRs (see Fig. 1) represents the most severe perturbation of a single-zone arrangement of fuel assemblies, and is a key feature related to the operation and safety of nuclear power plants.

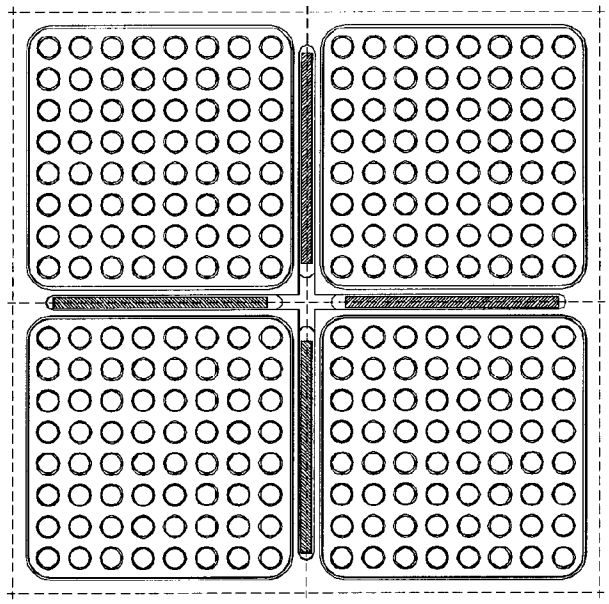

**Fig. 1:** Cruciform Absorber Blades in a BWR Lattice.

In this paper, the investigations related to the perturbation of an arrangement of Westinghouse SVEA-96+ fuel assemblies due to the presence of absorber blades corresponding to LWR-PROTEUS Phase I Configuration 2C are presented. This core configuration, described in Section 2, represented the irradiation of the lower part of the fuel assemblies under full-density water moderation conditions in the presence of boron carbide absorber blades.

The investigations have included scoping analyses, and the evaluation of CASMO-4 [3] and BOXER [4] capabilities using their corresponding *production models*. Special emphasis is given to two important reac-

tion rate distributions in the test assembly, and their variation due to the presence of the absorber blades. The first is the total fission rate ($F_{tot}$), closely related to the rod-by-rod $^{235}U$ depletion and important for the verification of operational limits associated with linear heat generation rates. In a controlled region, there is an overall power gradient from the furthest rod (in the sense of rod distance to the absorber blade vertex) to the closest rod. While the absorber blades are inserted, the total power developed by the perturbed assembly is rather low, but this strong gradient alters significantly the burnup distribution inside the assembly. This effect becomes important once the absorber blades are withdrawn later in the cycle to compensate for the core reactivity loss due to burnup. The second important integral parameter is the assembly distribution of the $^{238}U$ capture rate ($C_8$). The $F_{tot}/C_8$ distribution is somewhat depressed at the closest fuel rods. This is due, again, to the presence of the absorber blades, which are very efficient in absorbing thermal neutrons and thus hardening the spectrum locally. This effect is important since $C_8$ governs the build-up of plutonium, which is strongly modified in the fuel rods close to the absorber blades. This has an impact on the core excess reactivity, as well as on the shutdown worth of the blades. The distributions calculated with CASMO-4 and BOXER are given in Section 3.

As mentioned earlier, another object of investigation in the framework of the LWR-PROTEUS project is the sensitivity of *production models* to geometrical and materials characterization. The experimental nature of the studies allows the comparison of *production model* results (so-called *pre-calculations,* and directly related to the data used by the utilities) with results produced for the *ad-hoc*, specifically characterized system (the *post-calculations*). A significant effort was invested in the careful characterization of the fuel assemblies, and in the absorber blade geometry and material composition, taking into account the fuel vendor specifications and the typical departure from nominal conditions in densities, enrichments, tolerances and mechanical uncertainties. Section 4 describes a comparison of pre- and post-calculations obtained with BOXER for Configuration 2C. The results have demonstrated the reactor-physics sensitivity of modern BWR lattices to very small departures in the input data.

Section 5 presents the preliminary comparison of experimental (E) and calculated (C) values for $F_{tot}$ and $C_8$, as obtained with one deterministic code and the Monte Carlo code MCNP4C [5]. Finally, Section 6 is devoted to conclusions and recommendations.

## 2 LWR-PROTEUS DESCRIPTION

The zero-power, critical facility PROTEUS is unique: a central test tank, currently containing nine commercial BWR fuel elements, is "driven" critical and provides conditions which simulate different power reactor environments [6, 7]. During the year 2000, a series of measurements corresponding to full-water-density and voided-simulated neutron moderation conditions has been completed for the investigation of a Westinghouse SVEA-96+ fuel assembly. The investigations which have been carried out are representative of different enrichment and burnable-poison distributions in the fuel assemblies, considered over axially homogeneous regions as well as across an axial enrichment boundary.

The PROTEUS critical facility was configured in order to provide an appropriate LWR neutron spectrum environment to the centrally-located Westinghouse SVEA-96+ fuel assembly in which the measurements are carried out (the "test assembly"). The test assembly is surrounded by 8 other identical assemblies, the 3x3 arrangement being located inside an aluminium test tank. A view of the LWR-PROTEUS Core 2C test zone configuration is given in Fig. 2.

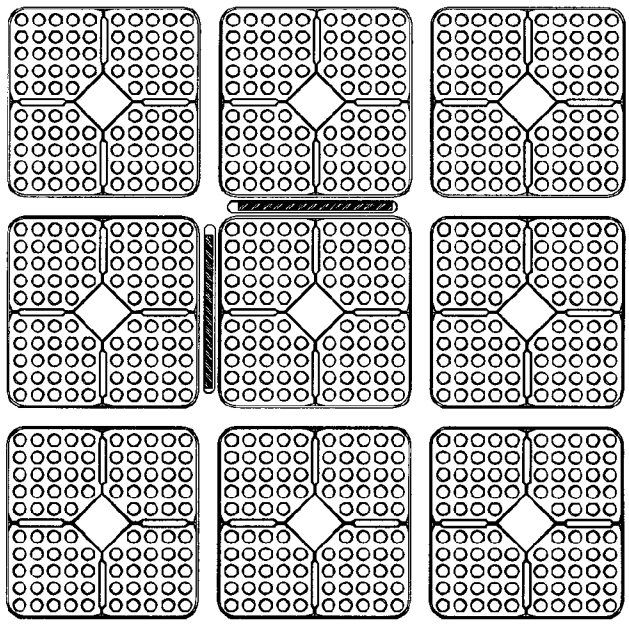

**Fig. 2:** Test Zone Configuration for LWR-PROTEUS Core 2C.

An SVEA-96+ fuel element comprises 96 fuel pins arranged in four separate sub-bundles, each containing 24 pins on a square pitch around a central water channel [8]. The $^{235}U$ enrichment varies both axially and radially in the range 2-5%, and some pins contain, additionally, gadolinium as a burnable poison in different concentrations (see Fig. 3). The lateral assembly dimensions are about 14 cm across.

Since the elements are 4.5 m in length and the active height of the PROTEUS driver regions is somewhat less than 1 m, the test tank can be driven axially to enable step-wise investigations along the whole length of the test assemblies. This is a special feature of the experiments, and is made possible by the unique layout of the facility. Thus, for example, it is possible to study the axial power profile variation across the axial enrichment boundary.

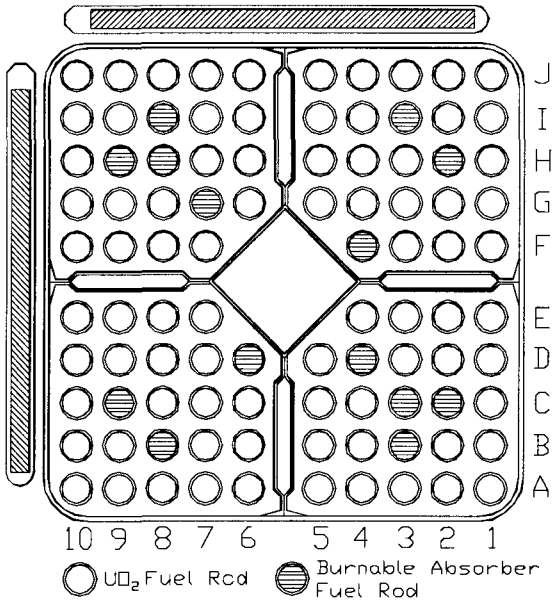


**Fig. 3:** Westinghouse SVEA-96+ Assembly Geometry.

The test tank is surrounded by outer radial regions [7] (the buffer, the $D_2O$-driver, the graphite-driver and a graphite reflector) which govern the reactor criticality, thus allowing experiments for a wide range of test lattice $k_\infty$ values. The reactor instrumentation channels, as well as the control and safety systems, are located in the outer regions, so that the experiments at the centre can be performed under "clean" conditions.

## 3 CASMO-4 AND BOXER PRE-CALCULATIONS

The basic system in Configuration 2C consists of a controlled assembly with reflective boundary conditions (see Fig. 3), which was studied in a manner representative of routine production calculations with CASMO-4 and BOXER. Built-in code default options and standard modelling were used, combined with input data based on nominal geometry and standard material compositions.

In the CASMO-4 calculations, thermal expansion and equilibrium xenon options were deactivated. The two-dimensional transport calculations were performed in 8 energy groups based on the default JEF-2.2 library with an extra energy boundary at 0.28 eV. In the BOXER calculations (Cartesian geometry), the central water channel was modelled as a square region with smeared Zircaloy and water; a similar procedure was used for the cruciform water wings. The Dancoff factors of the cells were corrected for the non-uniformity of the lattice (water gaps, etc.) using the energy-independent Monte Carlo option in BOXER (one average value for all rods of each cell type). For the two-dimensional transport calculations, the pins were modelled in the following way: corner pins were divided in a 3x3 mesh, other peripheral pins with a 3x1 mesh, and the remaining lattice pins with a single mesh per pin. The purpose of this refinement is to preserve the absorber blade geometry.

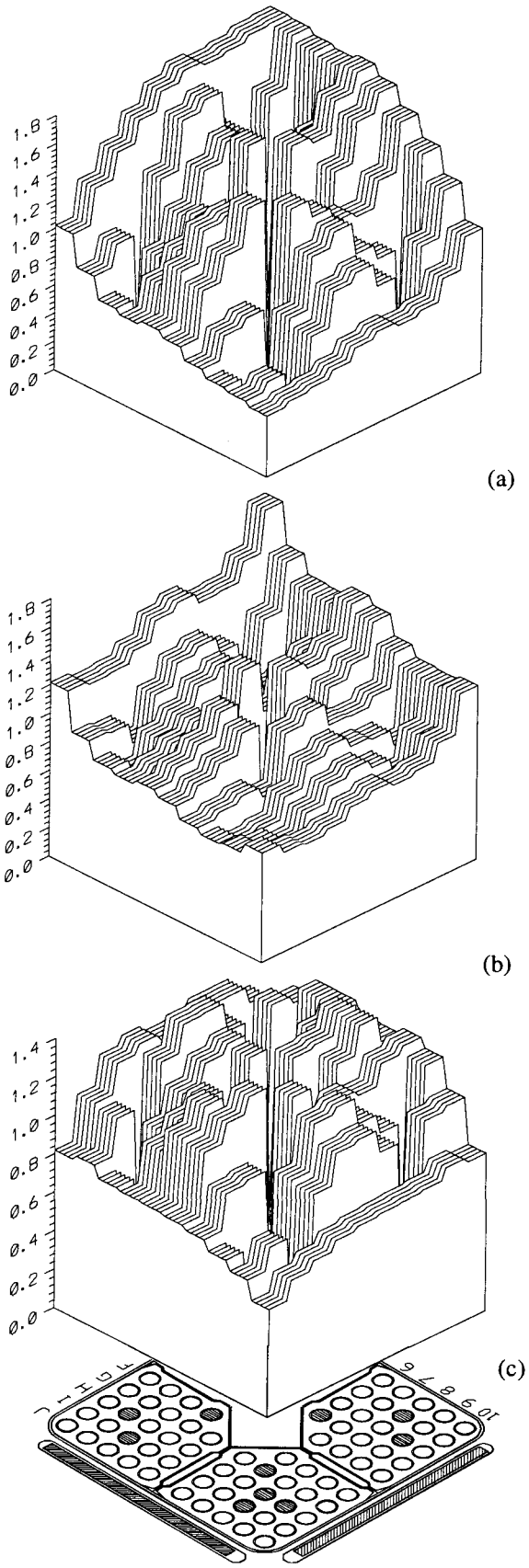


**Fig. 4:** Distribution of Average Integral Parameters for the Controlled SVEA-96+ Assembly: (a) $F_{tot}$, (b) $C_8$, and (c) the reaction rate ratio $F_{tot}/C_8$.

All CASMO-4 and BOXER results corresponded to the fundamental mode.

An illustration of both the strong lattice heterogeneity and the perturbation introduced by the absorber blades is derived from the CASMO-4 pre-calculations for this base case, as depicted in Fig. 4 for $F_{tot}$, $C_8$, and the ratio $F_{tot}/C_8$. Figures 4a and 4b show the different nature of the global reaction rate depression towards the absorber blades in the context, respectively, of thermal neutrons (governing $F_{tot}$), and of epithermal neutrons (largely governing $C_8$). Very clear as well is the strong heterogeneity imposed by the burnable absorber rods. Finally, Fig. 4c illustrates the reactivity-related effect on the rods close to the absorber blades (mainly, but not exclusively, the rods in row 'J' and column '10'). In these rods, $F_{tot}$ is relatively low and the $C_8$ high, indicating a relatively low consumption of $^{235}U$ and high production of fissile plutonium during irradiation.

The comparison of the CASMO-4 pre-calculations described in Fig. 4 and the corresponding BOXER results is given in Fig. 5. In the case of $F_{tot}$, significant differences are observed in the north-west sub-bundle, especially in the corner rod (rod J10) closest to the absorber blade vertex. This region of the assembly is one of the most difficult to estimate due, on the one hand, to the presence of the blades and, on the other, to the proximity of fuel rods to a gadolinium cluster (rods H8, H9 and I9). The overall flux depression towards the blades amplifies the sensitivity of this reaction rate to different approximations and models. In addition, other fuel rods in the gadolinium clusters show significant discrepancies (for instance, D3 and C4). Other discrepancies are rather small (within a few percent).

In the case of $C_8$, the overall agreement is better (a few percent on the average). The region with the most significant discrepancies extends over the north-west sub-bundle.

## 4 PRE- VS. POST-CALCULATIONS

The previous Section was devoted to illustrating the physics of controlled BWR assemblies, and to the description of typical discrepancies between different lattice codes for a well-characterized case. A high sensitivity has been observed for the calculated reaction rate distributions to different analytical treatments. Equally important is the evaluation of the sensitivity of the reaction rate distributions to departures from nominal conditions. By "nominal conditions" is meant the set of numerical values describing the necessary input for the reactor physics evaluation of the lattice. This consists of the "best-estimate" or standard values obtained from quality control and quality assurance files produced by the fuel vendor and the utility. The lattice characterization includes the definition of rod-by-rod fuel and cladding compositions (including uranium enrichments), and the fuel assembly geometry.

In practice, the real system departs slightly from the nominal data provided.

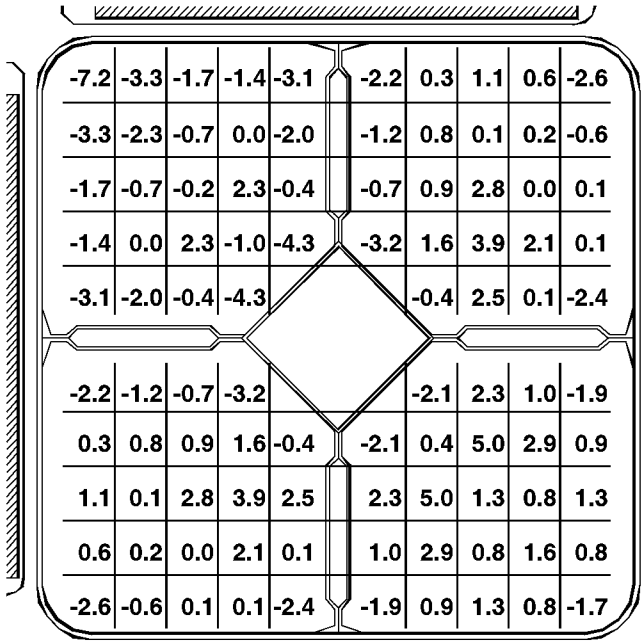


(a) $F_{tot}$

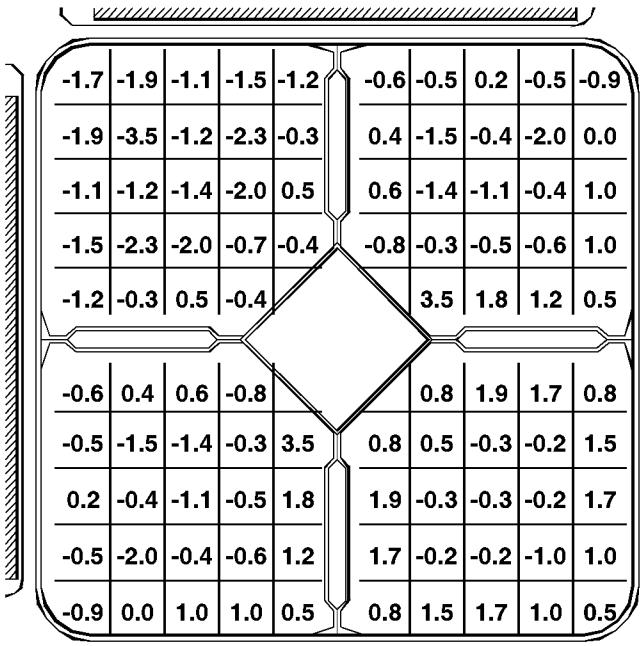


(b) $C_8$

**Fig. 5:** CASMO/BOXER-1 Results (in %) for (a) Total Fission Rate, and (b) $^{238}U$-Capture Rate.

For instance, the "measured" enrichments for a certain batch of fuel rods may depart by as much as 0.2% (relative). Other sources for departure from nominal conditions are associated with the mechanical fabrication of the fuel assemblies: for example, instead of being perfectly straight, an axial bending of as much as ~1 mm may be expected for the channels of fresh fuel assemblies.

The use of actual fuel assemblies in LWR-PROTEUS has brought the opportunity to study the sensitivity of integral parameters to typical departures from nominal. Using the measured material compositions provided by the fuel vendor, and the geometrical characterization performed in-house, post-calculational mod-

els have been developed and used for the comparision of calculations with the experimental data.

The effects of mechanical tolerances and real material compositions on the reaction rate distributions previously introduced have been evaluated using the code BOXER. In particular, the following characteristics departed very slightly from nominal conditions: $^{235}U$ enrichment, gadolinia content in burnable absorber fuel rods, horizontal length of the absorber in the blades, external dimensions of the blade, position of the blade (distance to its vertex and distance to the assembly), and position of the sub-bundles in the sub-channels. Figure 6 shows the percentage differences between post- and pre-calculations carried out with this code, i.e. for the two slightly different reflected-assembly models.

The main conclusion from this study is that the impact of typical departure from nominal conditions is larger than the discrepancies between the results produced by different codes for the same system. In the case of $F_{tot}$, discrepancies of about 10% were found in the corner rods, particularly in J10. Significant discrepancies were also found in the $UO_2$ rods close to the water channel, and in the peripheral rods close to the absorber blades. The discrepancies in $C_8$ are in general lower, but still significant. A sensitivity analysis is on-going to individualize the most important causes of these discrepancies.

## 5 EXPERIMENTAL VALIDATION IN CORE 2C

### 5.1 Fuel Rod γ-Scans in Configuration 2C

An automatic fuel rod γ-scanning machine was used to measure delayed γ-rays, from fission and activation, in individual fuel rods of the test assembly following irradiation in PROTEUS. The γ-scanning machine is a purpose-built, fully automatic device which enables the cyclic γ-scanning of activated fuel rods up to 4m in length [9] to be carried out. The machine consists of five main components: a 10-pin storage rack, a horizontal axis, a grab, a vertical-axis, and a measuring station.

The pneumatic grab transfers rods one by one along the horizontal axis to the measuring position and back. Once an individual rod is located in the measurement head, it is transported to the required vertical position by means of the vertical drive. The overall positional reproducibility is better than 1 mm. During measurement, the rod is rotated to eliminate the effect of azimuthal activity variations within the pin.

At the measurement position, there are two horizontally opposed germanium γ-ray detectors installed behind γ-ray collimators and shielding. The detectors are connected to EG&G Ortec DSPec devices combining a spectrometry amplifier and a multi-channel analyser, and employing digital signal processing to produce an optimum pulse shape, which gives good resolution and peak position stability over a wide range of count-rates.

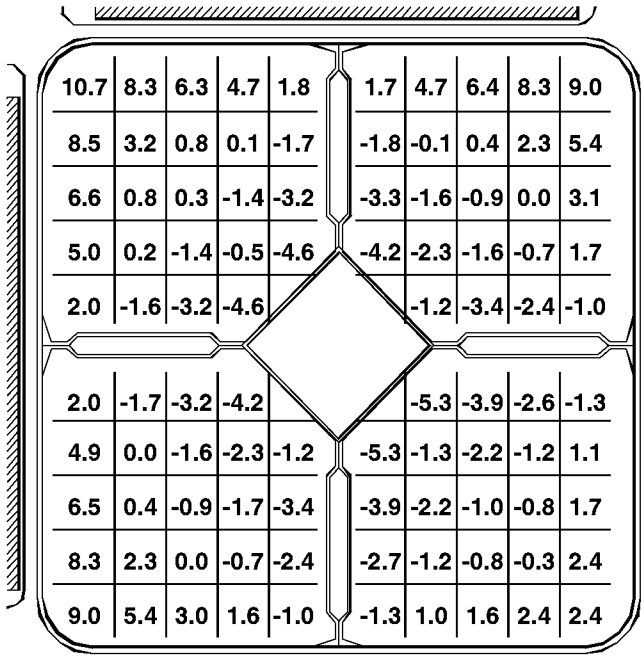


(a) $F_{tot}$

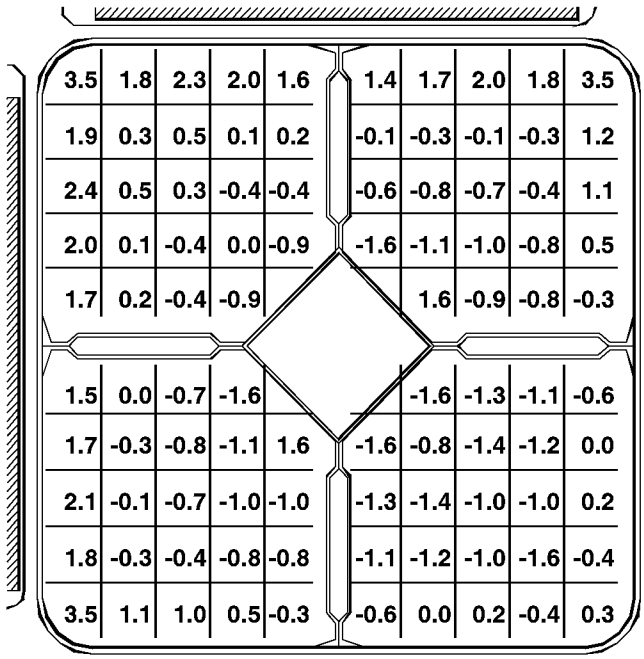


(b) $C_8$

**Fig. 6:** BOXER Post-/Pre-Calculation-1 (in %) for (a) Total Fission Rate, and (b) $^{238}U$-Capture Rate.

Six main γ-scanning measurements were made, each with ten fuel rods [10]. A final normalizing irradiation was carried out with selected rods from each of the previous six scans. The irradiations were timed as starting at 37% of the intended irradiation power, at a constant doubling time, and ending at reactor shutdown. A nominal power of 30 Watts and an irradiation duration of one hour were used for all of the γ-scan irradiations. Each spectrum collected was analysed; the background continuum was subtracted, peak areas were deconvoluted, nuclides were identified, and decay corrections were made.

### 5.2 Validation of Reflected-Test-Zone Calculations

The experimental results have been compared with calculational results from the deterministic code BOXER, and from the Monte Carlo code MCNP4C. For both codes, the reaction rates in the test assembly were calculated from a Reflected-Test-Zone (RTZ) model (as shown in Fig. 2) with reflective boundary conditions. A full-core model was also calculated with BOXER for the determination of correction factors accounting for outer-zone effects. The RTZ Monte Carlo calculations required 70 million neutron histories to achieve average 1σ statistical deviations of 0.42% for $F_{tot}$ and 0.76% for $C_8$.

Figures 7 and 8 show the distribution of (C-E), for the reaction rates obtained with BOXER and MCNP4C, respectively. Both calculated and measured distributions were first normalized to an average pin power of unity for the measured pins in the test element. The average (C-E) is thus zero for each of the considered distributions.

The comparison of the BOXER RTZ calculations and the experimental values reveals trends already identified from the pre- and post-calculations: i.e. explicable in terms of sensitivity to severe flux gradients. Thus, relatively large discrepancies are found for $F_{tot}$ in the fuel rods close to the blade vertex.

The most significantly perturbed rod (J10) shows a discrepancy of 6.6%. Other significant discrepancies (>4%) are observed in fuel rods close to this rod, such as J9 or I10, or some $UO_2$ fuel rods surrounded by two burnable absorber neighbours. In the case of $C_8$, the discrepancies are smaller, but nevertheless they show a clear trend for rod J10 and its neighbours.

The comparison of the MCNP4C RTZ calculations is qualitatively similar, and quantitatively somewhat better. The corner rod J10 also presents the highest $F_{tot}$ discrepancy. The distribution for $C_8$ is relatively more accurate. The most important statistical figures of merit corresponding to the deviations showed in Figs. 7 and 8 are compiled in Table 1.

Considering the high degree of heterogeneity of the SVEA-96+ fuel assembly, Table 1 indicates quite satisfactory agreement between the calculations and the measurements. In fact, analogous *rms* values found from the comparison of modern lattice calculations and experiments, for configurations *without* absorber blades (e.g. LWR-PROTEUS Configurations 1A and 1B), are very similar.

The reported calculation/experiment comparisons are currently being interpreted in greater detail. Thus, for example, the experimental conditions in the neighbourhood of the blade vertex are being reviewed. This may, at least partially, explain the relatively large discrepancies between some of the BOXER and MCNP4C results and the measured values.

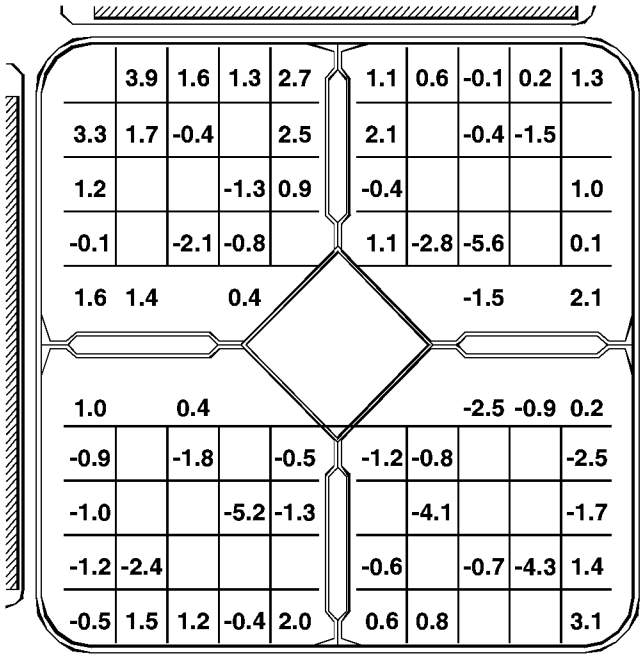


(a) $F_{tot}$

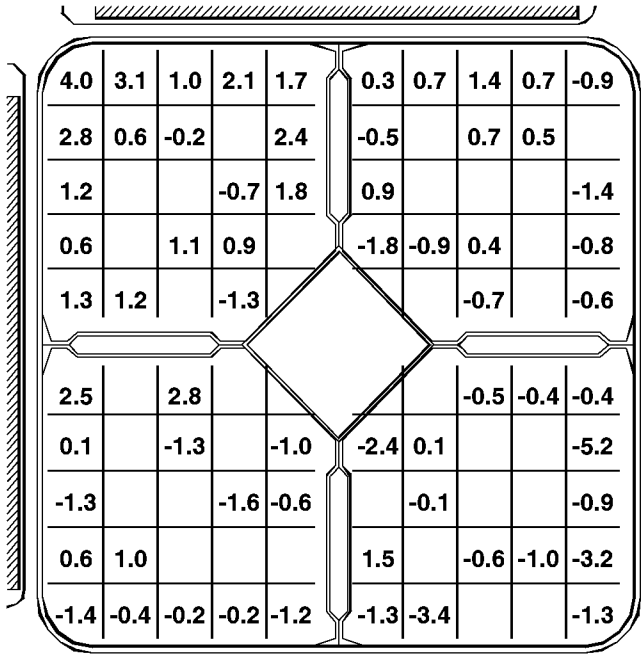


(b) $C_8$

**Fig. 7:** Distribution of 100x(C-E) obtained with BOXER using a Reflected-Test-Zone Model.

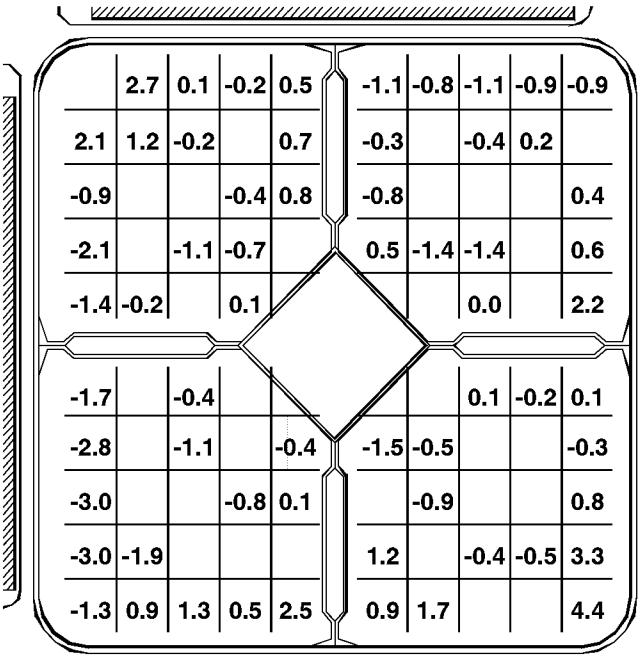


(a) $F_{tot}$

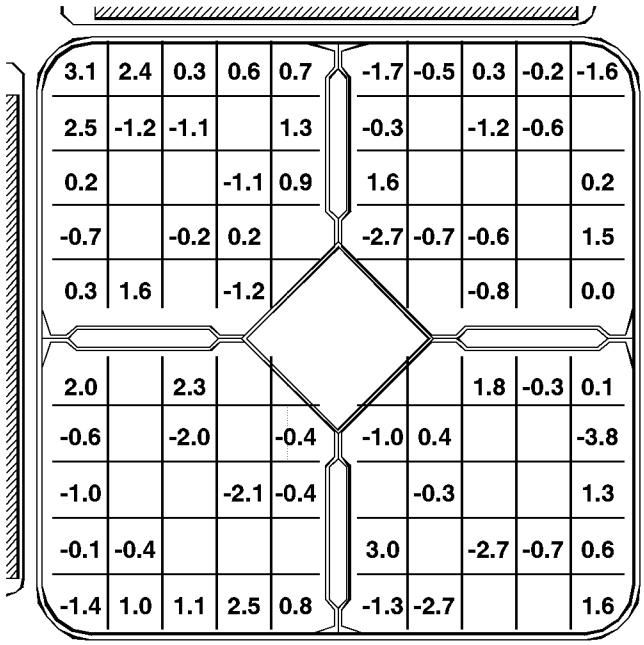


(b) $C_8$

**Fig. 8:** Distribution of 100x(C-E) obtained with MCNP using a Reflected-Test-Zone Model.

## 6 CONCLUSIONS

The paper describes the validation efforts invested for the qualification of modern calculational codes used in the determination of reaction rate distributions in a modern BWR fuel assembly strongly perturbed by the presence of boron carbide absorber blades.

Generally, the results of the performed calculations agree well with the measurements. The largest observed discrepancies appear to be localized on the corner rod where the most severe flux gradient occurs.

**Table 1:** Root-Mean-Square and Extrema for 100x(C-E) Reaction Rate Distributions in Core 2C.

| | BOXER | |
|---|---|---|
| *Parameter* | $F_{tot}$ | $C_8$ |
| *rms* | 2.1 | 1.6 |
| *max* | 6.6 | 4.0 |
| *min* | -5.6 | -5.2 |
| | **MCNP4C**[1] | |
| *Parameter* | $F_{tot}$ | $C_8$ |
| *rms* | 1.6 | 1.5 |
| *max* | 5.9 | 3.1 |
| *min* | -3.0 | -3.8 |

(1) Continuous-energy ENDF/B-V.

Thanks to the high-quality integral data being generated, and the flexibility of the PROTEUS facility, the current research project at PSI has aroused considerable international interest. This is the case for both utilities and fuel designers, all striving towards greater economy and improved safety margins.

## ACKNOWLEDGMENTS

The LWR-PROTEUS programme is being conducted jointly by PSI and the Swiss Nuclear Utilities, with specific contributions from Elektrizitätsgesellschaft Laufenburg (EGL) and Aare-Tessin AG für Elektrizität (ATEL). We are particularly grateful to H. Achermann (EGL), H. Fuchs (ATEL), W. Kröger (PSI) and G. Meier (KKG) for their strong support of the experiments. Thanks are also due to P. Bourquin, M. Berweger and R. Winter for excellent reactor operation and maintenance during 2000, as well as to J. Ulrich, J. Kohout and K. Kohlik of PSI's Logistics and Marketing Department (LOG) for their valuable engineering support.

## REFERENCES

[1] T. Williams, R. Chawla, P. Grimm, O.P. Joneja, R. Seiler, A. Ziver, *"New Experiments at a Zero-Power Facility Using Power Reactor Fuel",* Proceedings of the International Conference on the Physics of Nuclear Science and Technology, p. 720-727, Long Island, October 1998.

[2] T. Williams, *"Experimental Test Matrix for the BWR Phase (EGL/ABB) of the LWR-PROTEUS Experiments",* AN-41-98-04, Paul Scherrer Institut (1998).

[3] M. Edenius, K. Ekberg, B.H. Forssen, D. Knott, *"CASMO-4: A Fuel Assembly Burnup Program User's Manual",* Studsvik/SOA-95/1, Studsvik (1995).

[4] J.M. Paratte, P. Grimm, J.M. Hollard, *"ELCOS: The PSI Code System for LWR Core Analysis Part II: User's Manual for the Fuel Assembly Code BOXER"*, PSI Bericht Nr. 96-08, Paul Scherrer Institut (1996).

[5] J.F. Briesmeister, *"MCNP-A General Monte Carlo N-Particle Transport Code"*, LA-12625-M Version-4B, Los Alamos National Laboratory (1997).

[6] A. Ziver, T. Williams, P. Grimm, R. Seiler, *"Description of the Test Zone Components for the BWR Phase of the LWR-PROTEUS Experiment"*, TM-41-98-21, Paul Scherrer Institut (1998).

[7] A. Ziver, T. Williams, *"LWR-PROTEUS System Component Description"*, TM-41-98-07, Paul Scherrer Institut (1998).

[8] P. Andersson, *"KKL SVEA-96+/L Fuel Assemblies-Mechanical Design"*, BKB 94-020, ABB Atom AB (1994).

[9] M. Murphy, *"The LWR-PROTEUS Fuel Pin $\gamma$-Scanning Machine"*, Proceedings of the Annual Meeting on Nuclear Technology 99, ISSN 0720-9207, 425 (1999).

[10] M. Murphy, A. Lüthi, *"LWR-PROTEUS: The Results of Measurements in Configuration 2C"*. TM-41-00-06, Paul Scherrer Institut (2000).